

THE MULTIMUON SPECTROMETER

AT THE TEVATRON

A.V. Barnes, A.R. Clark, K.J. Johnson,
L.T. Kerth, S.C. Loken, T.W. Markiewicz,
P.D. Meyers, W.H. Smith, W.A. Wenzel

Physics Department and Lawrence Berkeley Laboratory
University of California
Berkeley, California 94720

M. Mugge and R.E. Shafer

Fermi National Accelerator Laboratory
Batavia, Illinois 60510

G.D. Gollin and F.C. Shoemaker

Joseph Henry Laboratories
Princeton University
Princeton, New Jersey 08544

Scientific Spokesman: S.C. Loken
Lawrence Berkeley Laboratory
(415) 486-6531
FTS: 451-6531

PROPOSAL SUMMARY

We propose to move the MultimMuon Spectrometer to the Tevatron muon beam. The distributed target-spectrometer magnet provides a high target luminosity (5 kg/cm^2) with high acceptance over the full target length. The detector is triggered in parallel by ≥ 1 , ≥ 2 , ≥ 3 muons in the final state using scintillation counter hodoscopes and calorimeter counters.

The initial physics objectives, to be measured simultaneously, are the following:

1. Measurement of weak-electromagnetic interference.
2. Inelastic muon scattering and determination of nucleon structure functions.
3. Production of high mass vector mesons.
4. Production of heavy quark states.
5. Heavy lepton production.
6. Study of final states with four or more muons.

We request 10 weeks of low intensity running to set up and test the apparatus. The initial physics objectives will require 65 weeks of running with the muon beam taking 20% of the accelerated protons.

I. Physics Objectives

A. Measurements of Weak-Electromagnetic Interference

Deep inelastic muon scattering at high Q^2 using muon beams of controllable helicity gives new and valuable information about the coupling of the neutral current to leptons and quarks.

A number of authors have explored the consequences of weak-electromagnetic interference¹. We assume for convenience that the sea contribution is negligible, the target is isoscalar and the x distribution of u and d quarks is identical; then the x dependence of the cross section is just that of the electromagnetic cross section.

With these simplifications, we can write the parity violating asymmetry

$$\frac{\sigma(\mu_R^+) - \sigma(\mu_L^+)}{\sigma(\mu_R^+) + \sigma(\mu_L^+)} = c Q^2 [G_V(g_L - g_R) - G_A(g_L + g_R) f(y)], \quad (1)$$

where

$$c = 8 \times 10^{-5} [\text{GeV}/c]^{-2},$$
$$f(y) = \frac{1 - (1-y)^2}{1 + (1-y)^2},$$

g_L , g_R are the left and right-handed couplings of the Z^0 to the muon and G_A and G_V are couplings to the quark. The couplings in 1 are specified in the Weinberg-Salam model²:

$$g_R = 2\sqrt{2} \sin^2 \theta_W$$
$$g_L = \sqrt{2} (-1 + 2 \sin^2 \theta_W)$$
$$G_A = -\frac{11}{12} \sqrt{2}$$
$$G_V = 2 \sqrt{2} \sin^2 \theta_W - \frac{11}{12}.$$

We take the value of $\sin^2 \theta_W$ from the polarized electron scattering experiment³,

$$\sin^2 \theta_W = .224,$$

so that

$$\frac{\sigma(\mu_R^+) - \sigma(\mu_L^+)}{\sigma(\mu_R^+) + \sigma(\mu_L^+)} = \frac{Q^2}{100 (\text{GeV}/c)^2} [0.008 + 0.002 f(y)].$$

At $Q^2 \sim 400 \text{ [GeV/c]}^2$ the parity-violating asymmetry is expected to be of order 3 to 4%.

The asymmetry

$$\frac{\sigma(\mu_L^+) - \sigma(\mu_R^+)}{\sigma(\mu_L^+) + \sigma(\mu_R^+)}$$

may be due both to two photon processes (which depend only on the muon charge and not on its helicity) and to weak-electromagnetic interference which does depend on the beam helicity. It is possible to sort out the two effects using their different dependences on y and Q^2 . The weak-electromagnetic asymmetry is given by

$$\frac{\sigma(\mu_L^+) - \sigma(\mu_R^-)}{\sigma(\mu_L^+) + \sigma(\mu_R^-)} = -cQ^2 \{2g_R G_A f(y)\} \quad (2)$$

which in the Weinberg-Salam model becomes

$$.013 f(y) \frac{Q^2}{100 \text{ (GeV/c)}^2} .$$

At $Q^2 = 400 \text{ (GeV/c)}^2$ this gives an asymmetry of 5% at $y = 0.9$.

The two-photon process alone is expected to give, using a combined light-cone and parton approach

$$\frac{\sigma(\mu_L^+) - \sigma(\mu_R^-)}{\sigma(\mu_L^+) + \sigma(\mu_R^-)} = \frac{\alpha}{\pi} \ln^2 \frac{Q^2}{M^2} \quad (3)$$

where M , a clothed parton mass, is not specified⁴. Taking the smallest mass consistent with the low Q^2 experiments⁵, we could choose $M > 640 \text{ MeV}$. This would yield asymmetries of order 10% at $Q^2 \sim 400 \text{ (GeV/c)}^2$.

The parity-violating asymmetry (Eq. 1) has been measured in polarized electron scattering at $Q^2 < 1 \text{ (GeV/c)}^2$ and the region $.15 < y < .36$ (see figure 1). The experiment proposed here will not significantly reduce the errors on the value of $\sin^2\theta_W$ but rather will make the following extensions:

1. Extend the region of y measured over the entire kinematic range. The proposed experiment has an acceptance rising with y , giving a nearly flat population in y . The expected coverage in y and relative errors are indicated in Figure 2.

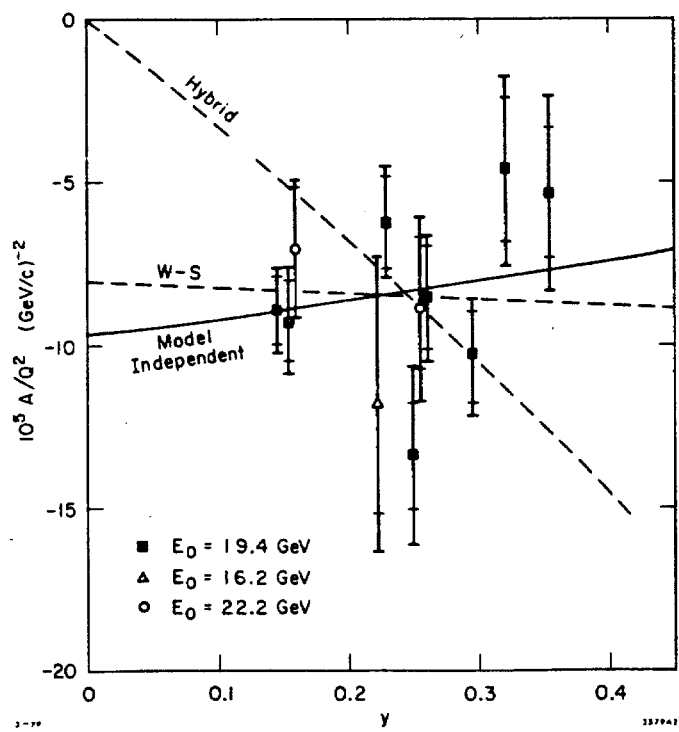


Figure 1. Measured asymmetry in polarized electron scattering (3).

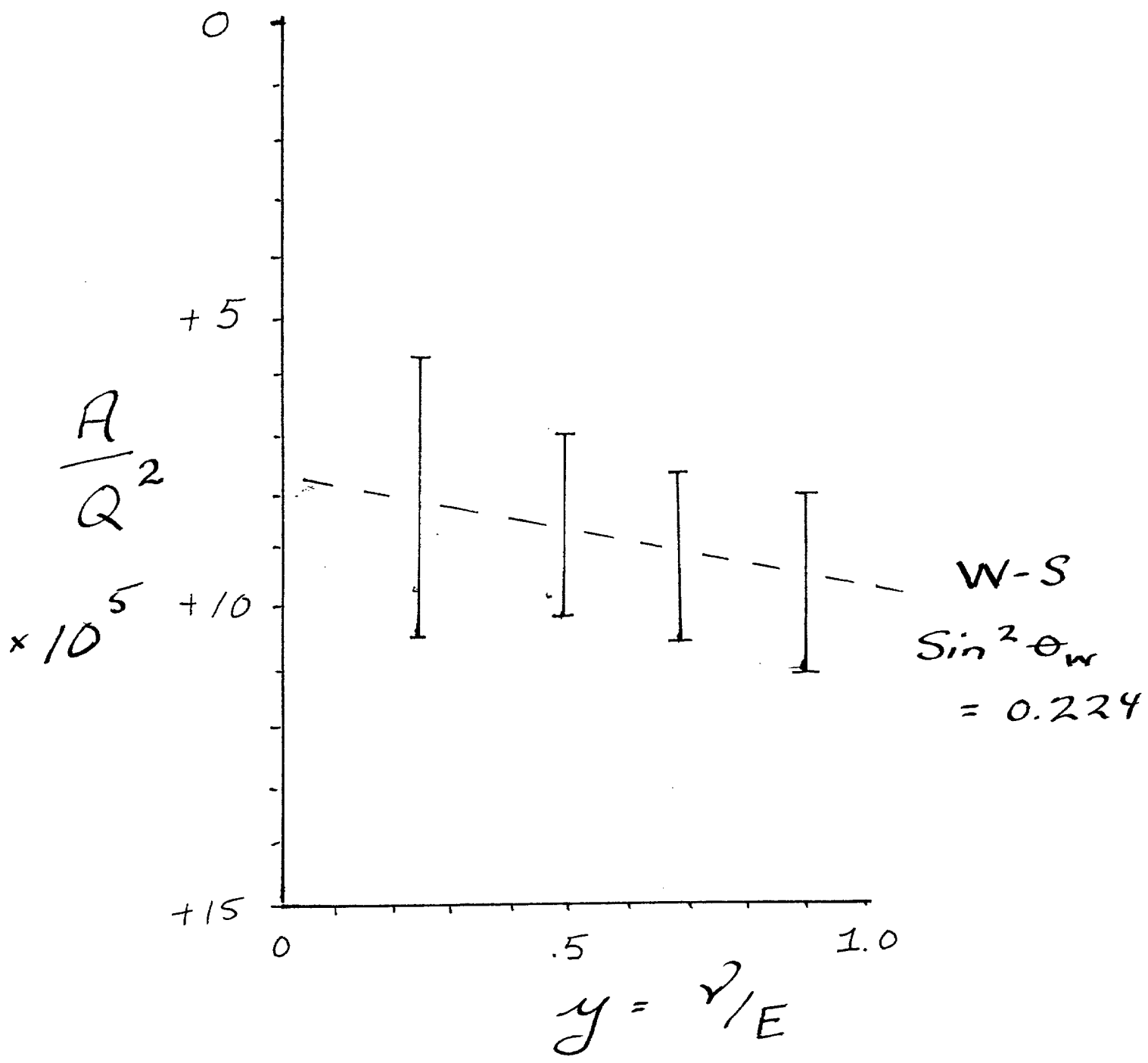


Figure 2. Expected errors as a function of $y=v/E$ for the proposed asymmetry experiment.

2. Extend the Q^2 range to $60 \leq Q^2 < 400$ [GeV/c]².
Although the Weinberg-Salam model does not suggest that the Z^0 couplings are Q^2 dependent, it is important to test this over a large kinematic region.
3. Extend the test to muon- Z^0 couplings. No tests of the muon coupling have been performed.

A measurement of the charge asymmetry (Equation 2) as a function of Q^2 and y is clearly of great interest. The two photon effect may be an important test of QCD⁶. The weak-electromagnetic interference will provide an independent linear combination of Z^0 couplings from those of the parity violating asymmetry. In particular, the so called "C violating" asymmetry gives a more sensitive handle on G_A , the axial coupling of the Z^0 to the quark, which one sees only in the small y slope of the parity violating asymmetry.

B. Inelastic Muon Scattering and Determination of Nuclear Structure Functions

The measurement of nucleon structure functions will continue to be of fundamental importance in our understanding of QCD. The MultimMuon Spectrometer provides the high luminosity required to extend this measurement to the highest possible values of momentum transfer. The distributed spectrometer magnet-target provides very high acceptance over the full length of the 5 kg/cm² target.

A detailed study of structure functions and in particular the investigation of high twist⁷ and higher order⁸ contributions will require data over the widest possible range in momentum transfer. In order to avoid regions of rapidly varying acceptance near the minimum scattering angle, these measurements must be made over a wide range in incident energy. Figure 3 shows the preliminary results on F_2 presented in 1979⁹. Table 1 summarizes the data which would be accumulated during the proposed running at 400 GeV and 600 GeV. Data will be taken at other energies to cover the full kinematic range accessible at the Tevatron.

This series of measurements will also permit the determination of $R = \sigma_L/\sigma_T$. This is an extremely important measurement which is invariably of limited precision because of systematic (not statistical) errors. We will continue to investigate how R may be determined with high precision. One possible technique which will be studied in detail is described in section VI.

C. Production of High Mass Vector Mesons

Data on the production of $J/\psi(3.1)$ by muons have been reported^{9,10}. Figure 4 shows the invariant-mass spectrum of $\mu^+\mu^-$ based on 50% of the data taken at 215 GeV. Monte Carlo simulation of the proposed run at 600 GeV shows that the mass resolution (9% at the ψ) will be unchanged from that at 215 GeV.

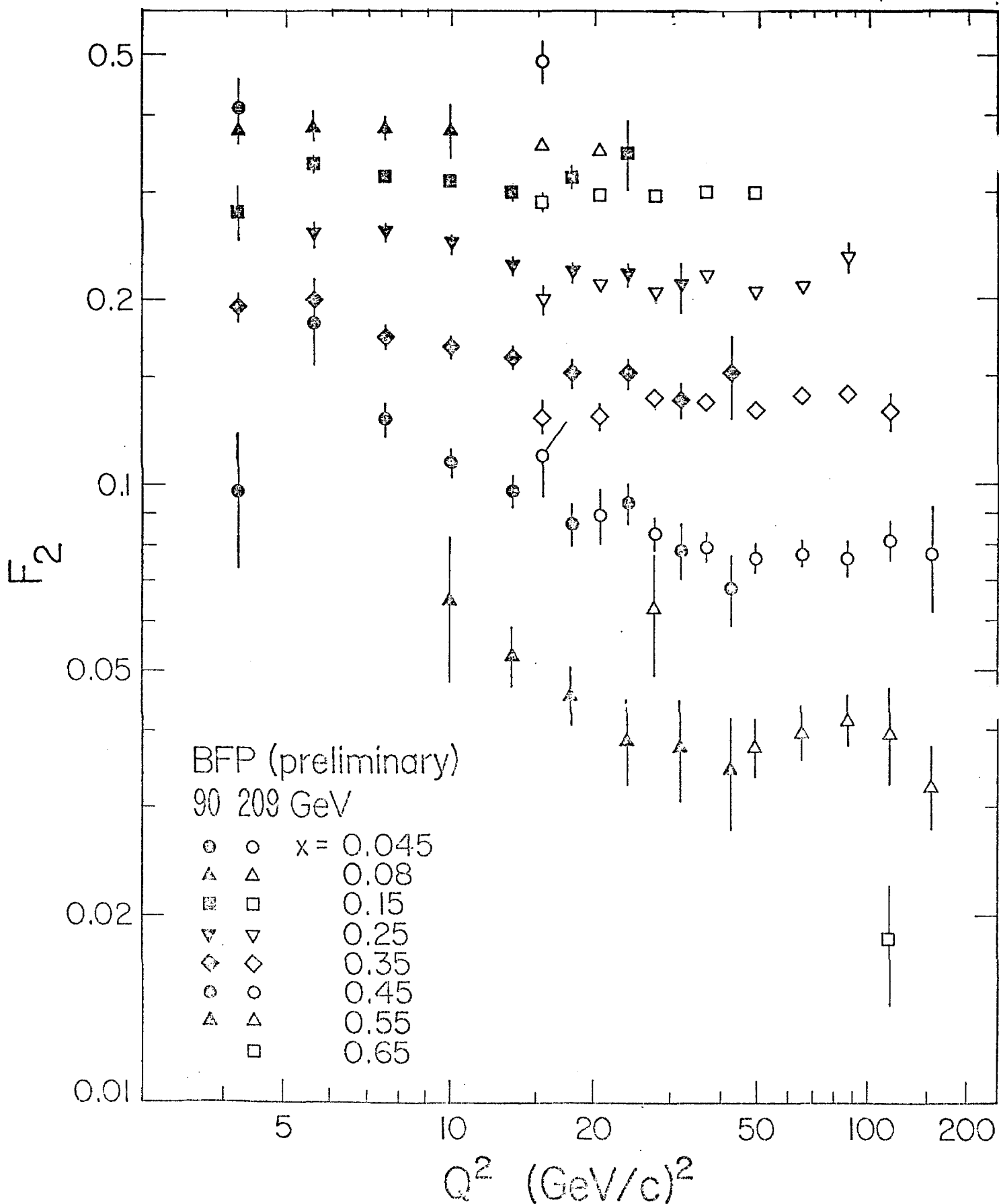


Figure 3. $F_2(x, Q^2)$, average for neutron and proton, measured in scattering of 209 GeV and 90 GeV muons from an iron target with nuclear effects removed. The value of $R = (1.6 - 0.7 Q^2)/(1.1 + Q^2)^2$ is assumed. F_2 is measured at the x values indicated, not the average x of data within a bin. The abscissa is linear in $\ln(\ln(Q^2/0.09))$. The errors indicated are statistical only.

Table 1

Inelastic Scattering Rates

| Q^2 | Events above this $Q^2/10^{12}$ Muons | |
|-------|---------------------------------------|-----------------|
| | E = 600 | E = 400 |
| 100 | 3×10^5 | 10^5 |
| 200 | 10^5 | 4×10^4 |
| 300 | 2×10^4 | 2000 |
| 400 | 5000 | 300 |
| 500 | 1000 | |
| 600 | 200 | |

EVENTS PER .026 GEV BIN

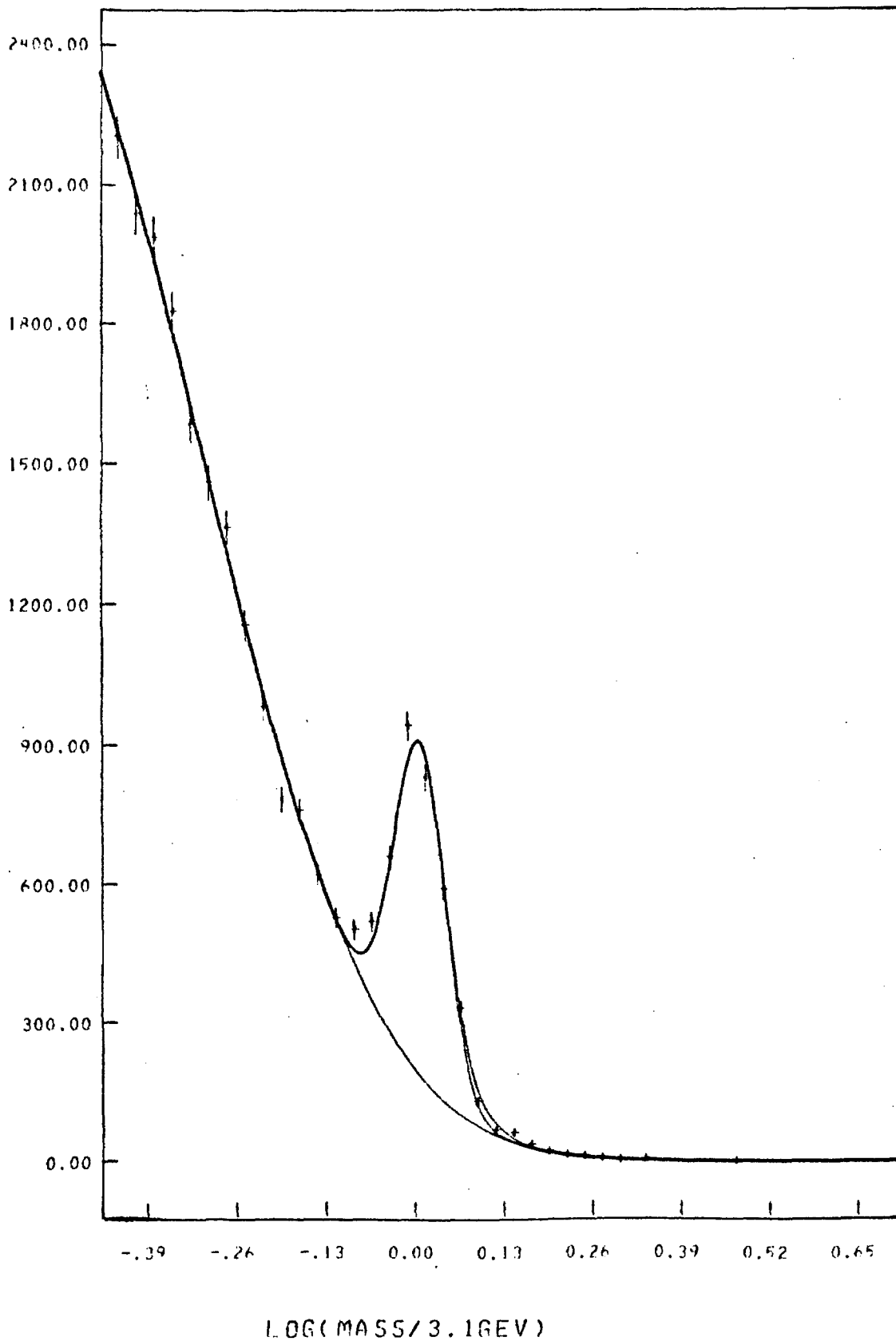


Figure 4. Invariant mass spectrum of $\mu^+\mu^-$ pairs produced by muons. The curve is a fit to $dN/dm_{\mu\mu} = g(u) \exp(f(u)) + h \exp(-u^2/(2(.09)^2))$ where $u = \ln(m_{\mu\mu}/3.1)$, f and g are quadratic and cubic polynomials in u , and $\exp(f(u))$ is a best fit to the continuum outside the ψ region.

We expect to see $\sim 50,000$ fully reconstructed elastic ψ 's for the proposed run at 600 GeV. Figure 5 indicates the kinematic range of these data.

The MultimMuon Spectrometer is a unique apparatus for the investigation of these 3 muon final states. The spectrometer has high acceptance even directly forward in the muon beam direction so that the virtual photon kinematics can be fully reconstructed.

Data taken at 215 GeV are in agreement with the QCD-based photon-gluon-fusion model¹¹. The high statistics of the proposed running will permit detailed comparison with this model and other QCD calculations.

The ψ decay angular distribution provides a handle on the ratio of longitudinal to transverse virtual photon cross sections. The tendency toward longitudinal absorption as Q^2 increases⁹ ($Q^2 > 2$) will be investigated in detail up to $Q^2 \sim 35$ (GeV/c)².

The increased statistics will also enable investigation of inelastic ψ production. As indicated in Figure 6, the data at 215 GeV show a significantly better signal to noise when we require the disposition of hadronic energy in the calorimeter. The inelastic sample does include ψ' cascades.

Production of the T (9.4) is expected to be suppressed relative to the ψ by a factor of order 100 even in the high energy limit¹². Data taken in this experiment will, however, permit a measurement of the cross section dependence on ν and Q^2 with statistics comparable to the early ψ results^{10,13}.

D. Production of Heavy Quark States

Data at 215 GeV show that 81% of the dimuon signal after basic cuts comes from forward charm production¹⁴. Background from π and K decay will be suppressed further at higher energies and the signal will be enhanced because of the higher average energy of the outgoing muons.

For a run of 2×10^{12} incident muons at 600 GeV, we would accumulate in excess of 10^6 fully analyzed charm decays. As indicated in Figure 7, these cover the full kinematic range in ν accessible in the beam and extend above $Q^2 \sim 50$ (GeV/c)².

These data will be extremely valuable for the detailed study of photon-gluon-fusion and other QCD models¹⁵. In addition the data are of fundamental importance in understanding measurements of the nucleon structure functions. In the photon-gluon-fusion model, the quarks couple to the nucleon via a gluon (Figure 8). Thus, the process is not sensitive to the quark content of the nucleon but it contributes to the virtual

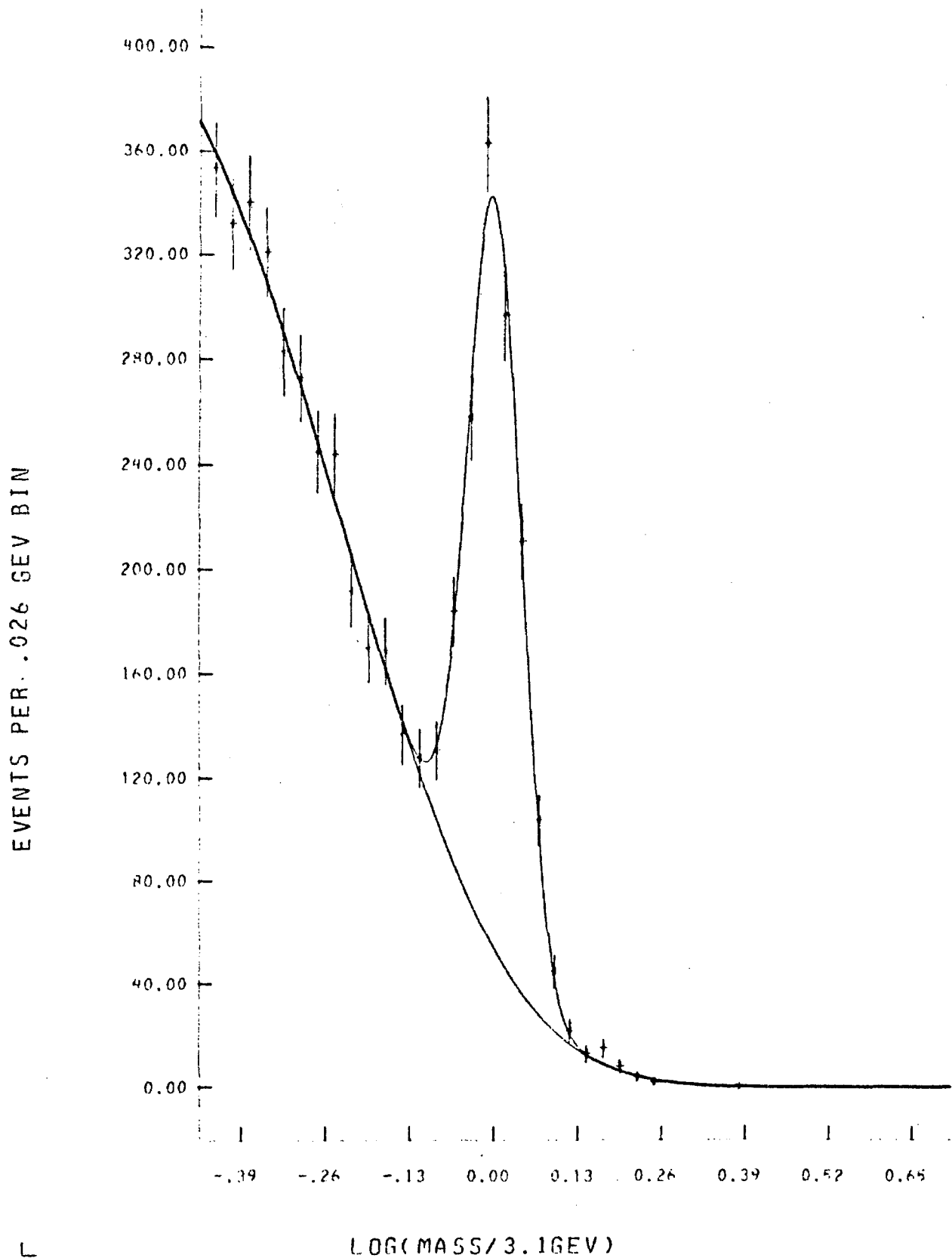


Figure 6. Invariant-mass spectrum for the events in Figure 3 which satisfy the criterion for inelastic production based on hadronic energy deposited in the calorimeter. This sample includes ψ' cascades.

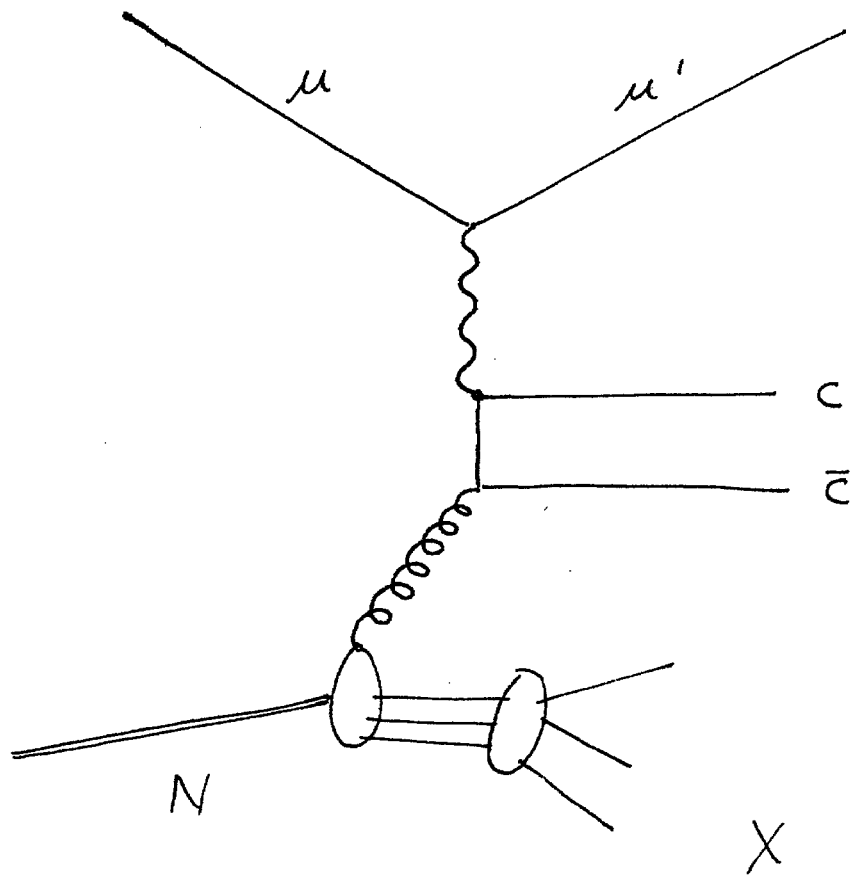


Figure 8. Production of charmed quarks by photon-gluon-fusion.

photon total cross section as included in the structure function . In particular, the process violates scaling with strong dependence on both Q^2 and ν so that QCD analysis of the structure functions must include this contribution.

Production of b quarks is again suppressed¹² . Monte Carlo simulation indicates that it will be extremely difficult to resolve the b signal from under the dominant c "background". The study of multimueon events from cascades will give additional handles on the production of heavier flavors.

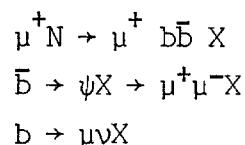
E. Heavy Lepton Production

Experiment 203 was proposed as a search for a right-handed neutral heavy lepton predicted by gauge theories. One early argument for the existence of the M^0 , the "hybrid" gauge model, is disfavored by the SLAC-Yale measurement³.

Limits on production of neutral and doubly charged heavy leptons by 215 GeV μ^+ are indicated in figure 9 . These limits correspond to an earlier analysis of 20% of the data⁹. The limits are obtained by the study of events with high Q^2 and high p_{\perp} relative to the assumed virtual photon. The running proposed here will significantly improve the sensitivity of the heavy lepton search. In addition, a similar sensitivity can be achieved for leptons with a V-A coupling during the running of the helicity asymmetry.

F. Study of Rare Muon Induced Processes

Rare events are defined as those having ≥ 4 muons or 2 missing leptons in the final state. The properties of 4 rare events found in a preliminary scan of 20% of the E203/391 data have been described⁹. In particular, the event depicted in Fig. 10 is interpreted as



The estimated background is less than 10^{-3} events⁹.

Further analysis has located 13 4 muon events and 11 events with 5 outgoing muons. The properties of these events are presently under study. The multimueon detector provides measurement of all muon energies and transverse momenta, as well as determining Q^2 , ν , the total hadronic energy and the missing energy in the reaction.

The proposed running will significantly increase the sample of rare events. For example, we would expect ~ 50 of the $b \rightarrow \psi$ cascades as in Figure 10.

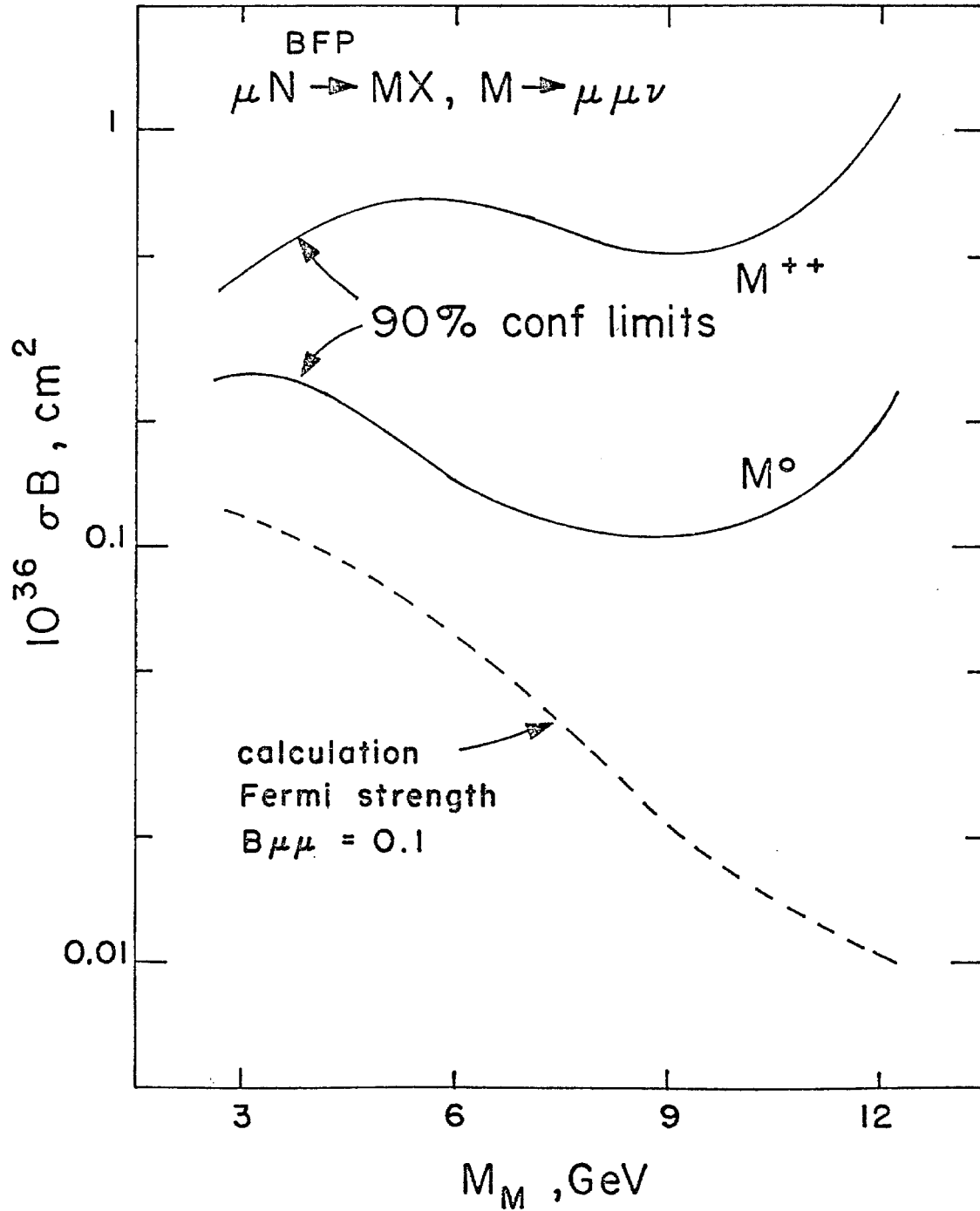


Figure 9. 90% confidence limits on production by 209-GeV μ^+ of neutral and doubly-charged heavy leptons of mass M_M decaying to $\mu\nu$. If the beam muon were coupled to such leptons by a right-handed weak current of Fermi strength and if the $\mu\mu\nu$ branching ratio were 0.1, the signal level would be that indicated by the dashed line.

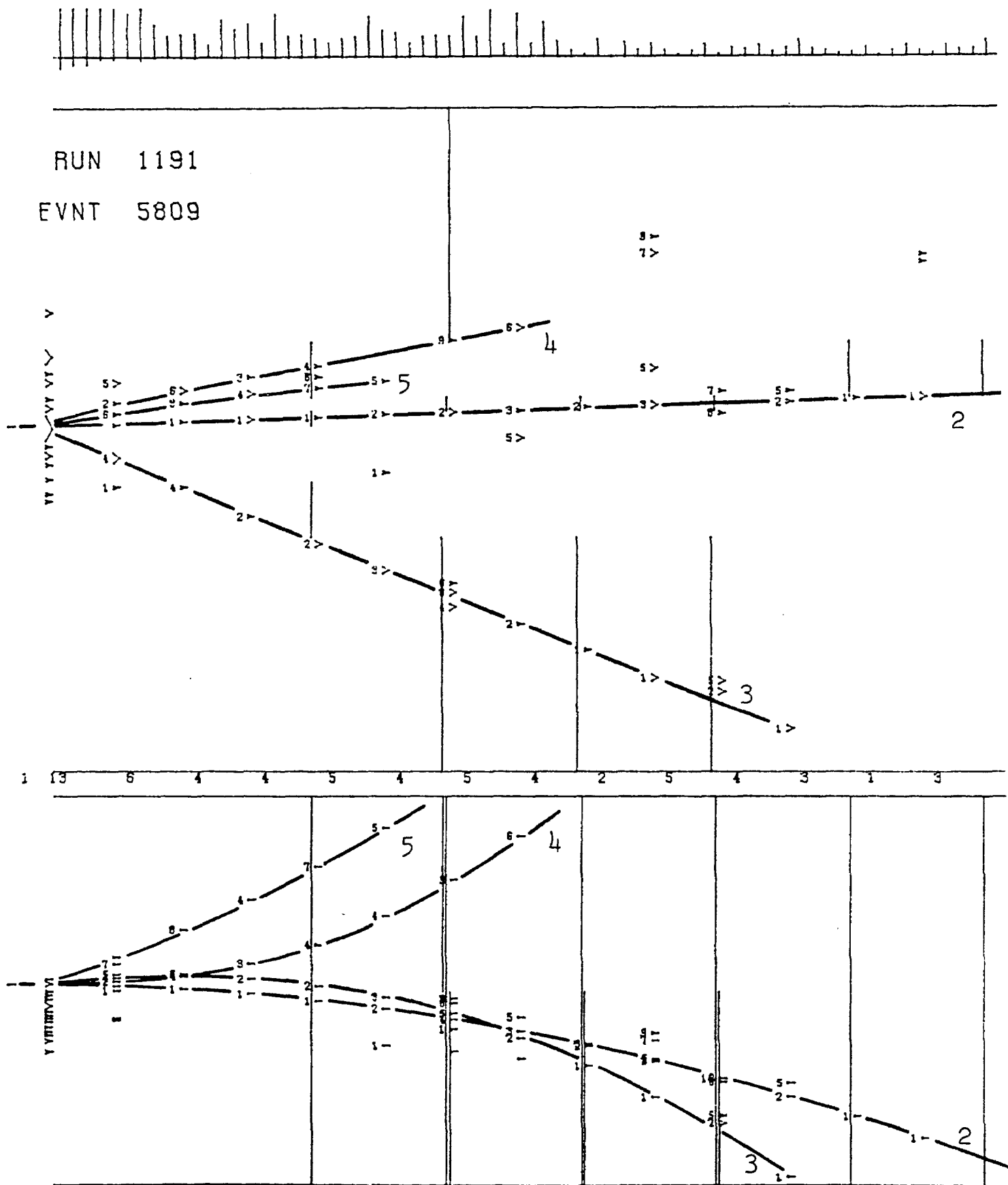


Figure 10. Computer drawn view of 4 muon event. The superimposed digits are program assigned track numbers. Typically, in each interstices between modules, a track registers in a proportional chamber (left tic) and drift chamber (right tic closest to left tic). The drift chambers are noisier because of their longer memory. Short vertical lines at the top are calorimeter pulse heights. Long vertical lines are projections of counters which were tagged. Heavy broken lines are tracings of the computer-reconstructed trajectories.

III. Experimental Procedures

To measure the parity violating asymmetry (IA) we will hold the muon beam momentum constant while varying the hadron beam central momentum so as to accept primarily forward or background pion decays. The optimum muon beam momentum for this measurement will depend on the details of the final muon beam design.

We have studied the optimization of a naive figure of merit (yield² x average polarization) for the preliminary beam design¹⁷. This study shows a rather broad optimum and we are inclined to move conservatively towards larger average polarization so as to reduce systematic uncertainties.

To minimize time dependent systematic effects in the apparatus it is desirable to vary the beam helicity as often as possible. Our ability to make these changes will depend on the beam design and we will work closely with the Neutrino Department to develop an efficient solution. One possible scenario would be to interrupt the Tevatron flat top for pulses to the Bubble Chamber and neutrino detectors. During that time the hadron beam momentum could be changed (typically by a factor ≤ 2). With many such pieces of the flat top, the polarization could be randomly varied.

A measurement of the decay electron energy spectrum provides a determination of the average polarization (Figure 13). The background to this measurement from muon bremsstrahlung can be suppressed by requiring $E_e/E_\mu \leq .9$ and vetoing on muons emerging from the shower detector. We have also studied the use of a magnetized iron polarimeter. While the signal here is extremely small, preliminary calculations indicate this may be useable as an additional polarization monitor.

The charge asymmetry (IB) can be carried out at all muon beam energies. The multimMuon spectrometer is charge symmetric. In addition, the spectrometer will be reversed periodically to reduce systematic bias in the detector.

During the running of measurements IA and IB, we will also trigger on all multimMuon events (I(D, E, F, G). The reversal of muon charge and the spectrometer magnetic field are extremely important in ensuring that the multimMuon acceptance is charge symmetric.

Table 3 indicates a tentative allocation of running time based on preliminary beam designs.¹⁷ This allocation will, of course, be subject to change as the design parameters are defined. In addition, physics priorities at the time of running will determine running time allocation.

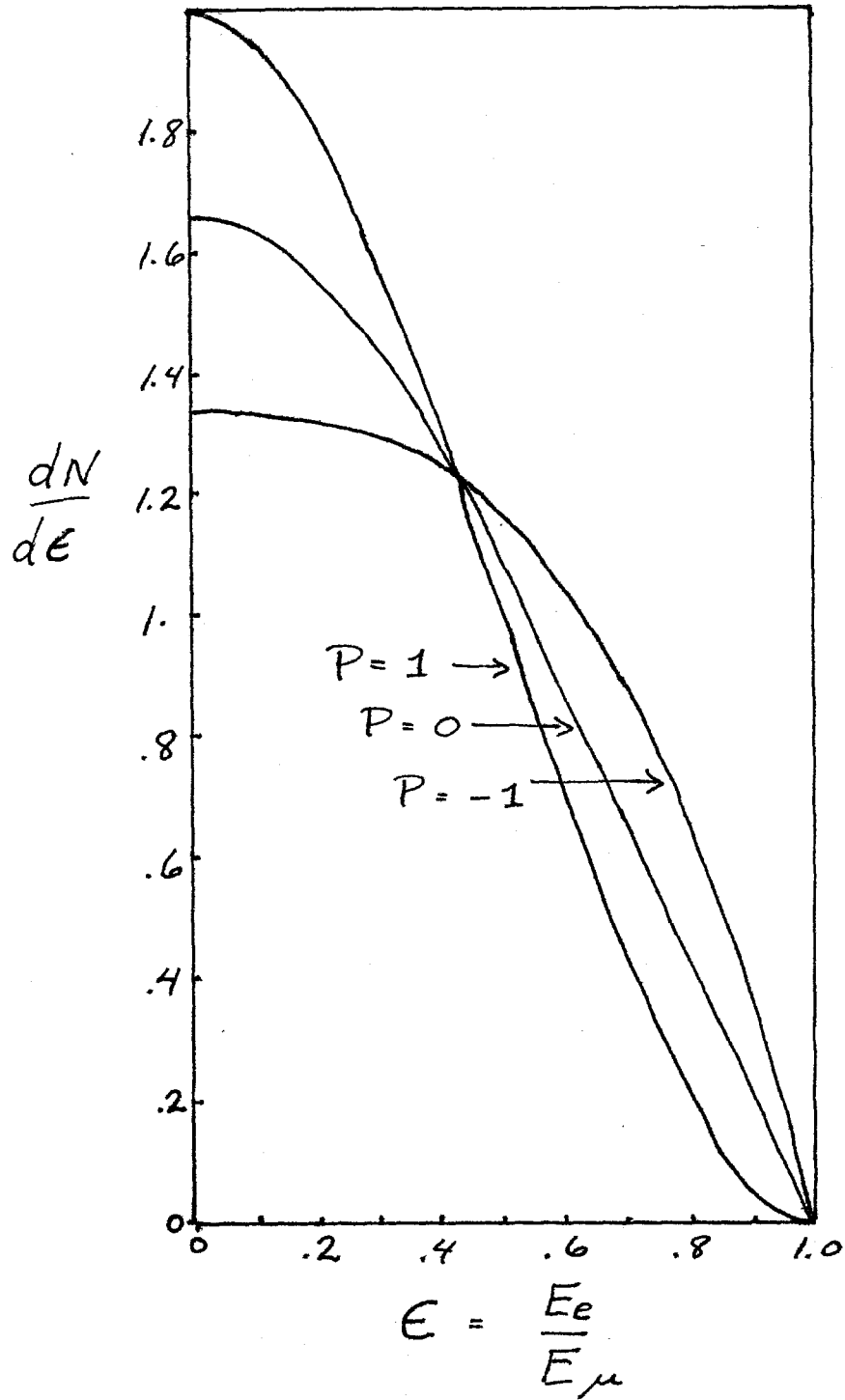


Figure 13. Electron energy spectrum from muon decay in flight for 3 values of muon polarization.

II. Apparatus

The MultimMuon Spectrometer is shown schematically in Figure 11. It consists of 18 25-ton modules each containing 5 10-cm thick steel plates, 5 calorimeter scintillators (omitted in modules 16-18) and a pair of proportional (PC) and drift chambers (DC). Banks of 12 trigger scintillators (S_1 - S_{12}) are located in even modules 4-18.

The fiducial volume, $1.8 \times 1 \text{ m}^2$ in area extends 16 m in the beam direction. Within the central $1.4 \times 1 \text{ m}^2$ area of each magnet plate, the 19.7 Kgauss field is uniform to 3% and mapped to 0.2%. Appendix A describes the magnet design and measurement in detail.

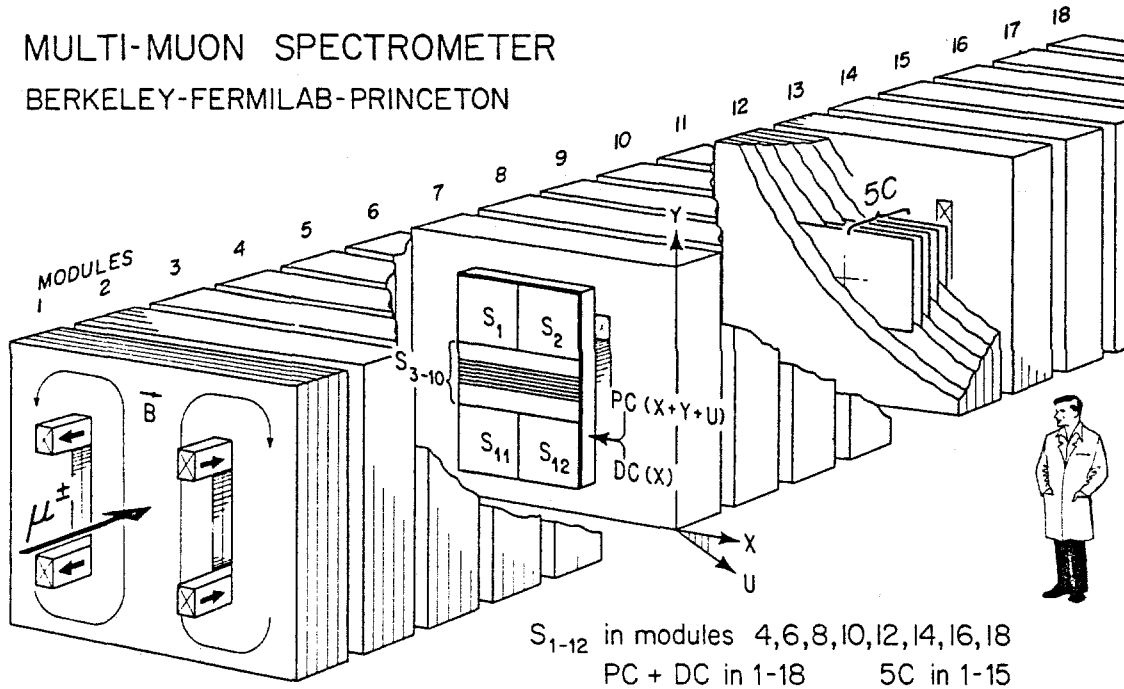
Figure 12 is an exploded view of the detectors in the gap downstream of each module. The 2 cm drift chamber cell and specially designed readout electronics make possible a system efficiency exceeding 98% during high rate ($< 10^7$ particle/sec) conditions¹⁶. Twofold DC ambiguities are resolved by the PC anode wires spaced at $\Delta X = 3 \text{ mm}$. Coordinates at 30° (u) and 90° (y) to the bend direction are registered by means of the 5 mm wide cathode strips (see Appendix B).

The spectrometer is triggered in parallel by ≥ 1 , ≥ 2 , or ≥ 3 muons in the final state. The required signatures in the scintillator hodoscopes and calorimeter counters are listed in Table 2. The multimMuon triggers can not be vetoed by hodoscope and calorimeter information; the $\geq 1\mu$ and $\geq 3\mu$ triggers are affected in no way by the calorimeter signals. Under some conditions when more than one count is required from a scintillator hodoscope, two of the contributing hodoscope elements are required to be non-adjacent.

To suppress accidental multimMuon triggers, the trigger logic is vetoed by halo muons in the same RF bucket, or beam muons in the same or adjacent buckets. In the existing muon beam this logic induces a deadtime which ranges up to 50%.

The trigger system is designed to suppress accidental multimMuon triggers caused by multiple small showers along the muon track. Each trigger hodoscope is bolted to the downstream face of the magnet plate so that the spatial extent of showers emerging from the iron is reduced. In the downstream 1 or 2 banks in the trigger, the multimMuon hits are required to be non-adjacent. The trigger requires a multimMuon signature in each of 3 consecutive trigger banks with 1 meter of iron between consecutive banks. To suppress accidental triggers further at high muon energy we will add additional banks in the odd gaps. This modification will not reduce the acceptance for good multimMuon events.

MULTI-MUON SPECTROMETER
 BERKELEY-FERMILAB-PRINCETON



XBL 795-9605

Figure 11. Schematic view of the apparatus. The solid dipole spectrometer magnet serves also as a target and hadron absorber. S_1 - S_{12} are trigger scintillators (1 of 8 banks). DC and PC are 1 of 19 pairs of drift and proportional chambers. Each proportional chamber measures projections on three coordinates. The scintillators labelled 5C are 5 of 75 counters performing hadron shower calorimetry.

V. Time Scale and Other Commitments

We believe that the new muon beam can and should be operational by late 1983. The new muon laboratory should be ready approximately 1 year before the beam is commissioned so that the apparatus can be installed.

The senior physicists at LBL are now committed to the Time Projection Chamber at PEP. This will begin data taking in early 1981. If the muon beam proceeds on the time scale above, this proposal will be the principal research activity of the LBL group beginning in mid-1982.

M. Mugge will begin to work for the Neutrino Department and will be deeply involved in the development of the new muon beam. R. Shafer has no other experimental commitments.

F. Shoemaker is participating on Fermilab experiment 615 which will run in early 1982. Beyond that time, this proposal will be his principal commitment.

The four graduate students on the experiment (3 at LBL and 1 at Princeton) wish to work on this proposal. This involvement will, however, depend on where they go after completing their theses.

LBL and Princeton will add post-doctoral physicists and graduate students (2 at LBL and 1 at Princeton) to maintain at least the level of E203/391.

In the next section, we discuss the development of new hardware to enhance the capability of the detector. If we pursue this as an additional proposal, we expect to add new institutions to the collaboration.

VI. Future Plans

The MultimMuon Spectrometer provides a uniquely versatile detector for the study of single muon and multimMuon final states up to 1 TeV. We will continue to investigate how the detector can be improved for use at the Tevatron. At the present time our attention is focused on the possibilities for an enhanced calorimetric detector which could be installed upstream of the magnetic spectrometer.

A number of calorimetric detectors have been developed which allow determination of both shower energy and direction¹⁸. In addition, it is possible to use the second moment of the shower angular distribution to extract the invariant mass of the hadronic system. The measurement of shower development in a fine grained calorimeter permits the separation of hadron and electron induced showers.

We will continue to examine possible detector designs and develop a calorimeter optimized for use in the muon beam. The physics motivations for such a new detector are many:

1. Inelastic scattering kinematics can be determined by the use of calorimetric information alone. Use of the total energy ($\sim \nu$) and the second moment ($\sim W^2$) will determine the kinematics of inelastic scattering independently of the scattered lepton. The detector efficiency and resolution, then, need not depend on incident energy. Such a detector offers the possibility of providing an independent determination of $R = \sigma_L/\sigma_T$ with completely different (and hopefully smaller) systematic errors.
2. Higher resolution measurements of energy and direction will provide additional constraints on the analysis of multimMuon events.
3. The detector could be used for the study of jets produced in inelastic scattering.
4. The detector provides a measurement of the decay electron energy spectrum needed for the measurement of beam polarization.
5. The measurement of inelastic scattering kinematics with no outgoing muon provides a unique probe of V+A charged current weak interactions. Present limits on the mass of a right-handed W boson¹⁹ ($M_{WR} > 2.8 M_{WL}$) would still permit a signal at approximately 1% of the V-A rate. A measurement at this level appears feasible at Tevatron energies. Charged current weak interactions contribute $\sim 20\%$ ν^2 relative to electromagnetic interactions ($\nu = Q^2/2ME$). For a μ^+ beam V+A is enhanced by a flat y distribution relative to $(1-y)^2$ for V-A. Preliminary calculations indicate that backgrounds from muon decay and catastrophic energy loss can be managed with a calorimeter of sufficient angular resolution.

We expect to present a proposal for such a detector upgrade as our design calculations are completed.

Table 3

Tentative Allocation of Running Time

| Beam | N_{μ} | Yield (Ref. 17) $\mu/\text{interacting } 800 \text{ GeV proton}$ | N_p^a on target | Weeks ^b |
|-----------|---------------------|---|----------------------|--------------------|
| 600 GeV | | | | |
| μ^+ | $.5 \times 10^{12}$ | 10^{-5} | 1.4×10^{17} | 20 |
| μ^- | $.5 \times 10^{12}$ | $.5 \times 10^{-5}$ | 2.7×10^{17} | |
| 400 GeV | | | | |
| μ_L^+ | 10^{12} | 4×10^{-6} | 7×10^{17} | 45 |
| μ_L^- | 10^{12} | 2×10^{-5} | 1.5×10^{17} | |
| μ_R^+ | 10^{12} | $.5 \times 10^{-5}$ | $.5 \times 10^{17}$ | |

^a We assume 1/e of protons interact.

^b These estimates assume 10^{17} protons accelerated/week with 20% of these going to the muon beam.

IV. Effort and Resources Required

The Multimuron spectrometer must be moved from its present location to the new muon beam. We will request Fermilab rigging support for this move. The apparatus is welded into 18 25-ton modules which could be moved as units. We estimate the moving of the magnet will require 4-6 weeks once instrumentation is removed.

The experimenters will move all sensitive detectors. In addition, optical alignment of the magnet and detectors during installation will be the responsibility of the experimenters.

We expect to do some reworking of the detector systems to improve performance in the new beam. In particular, one of the large proportional chambers is being studied now at LBL (see Appendix B). Additional scintillator trigger banks will be added to reduce accidental multimuron triggers and improve acceptance uniformity.

We will use Prep electronics for all fast logic and the hardware required would be comparable to that used in the running of E203/391 in 1978. (see Appendix C).

The Princeton PDP-15 has been removed and we will request an on-line computer system from LBL Physics Division or the Fermilab computing department.

We expect the Fermilab Neutrino Department to provide beam line instrumentation. We will work closely with the Fermilab physicists to develop this instrumentation and to interface it to our data acquisition system.

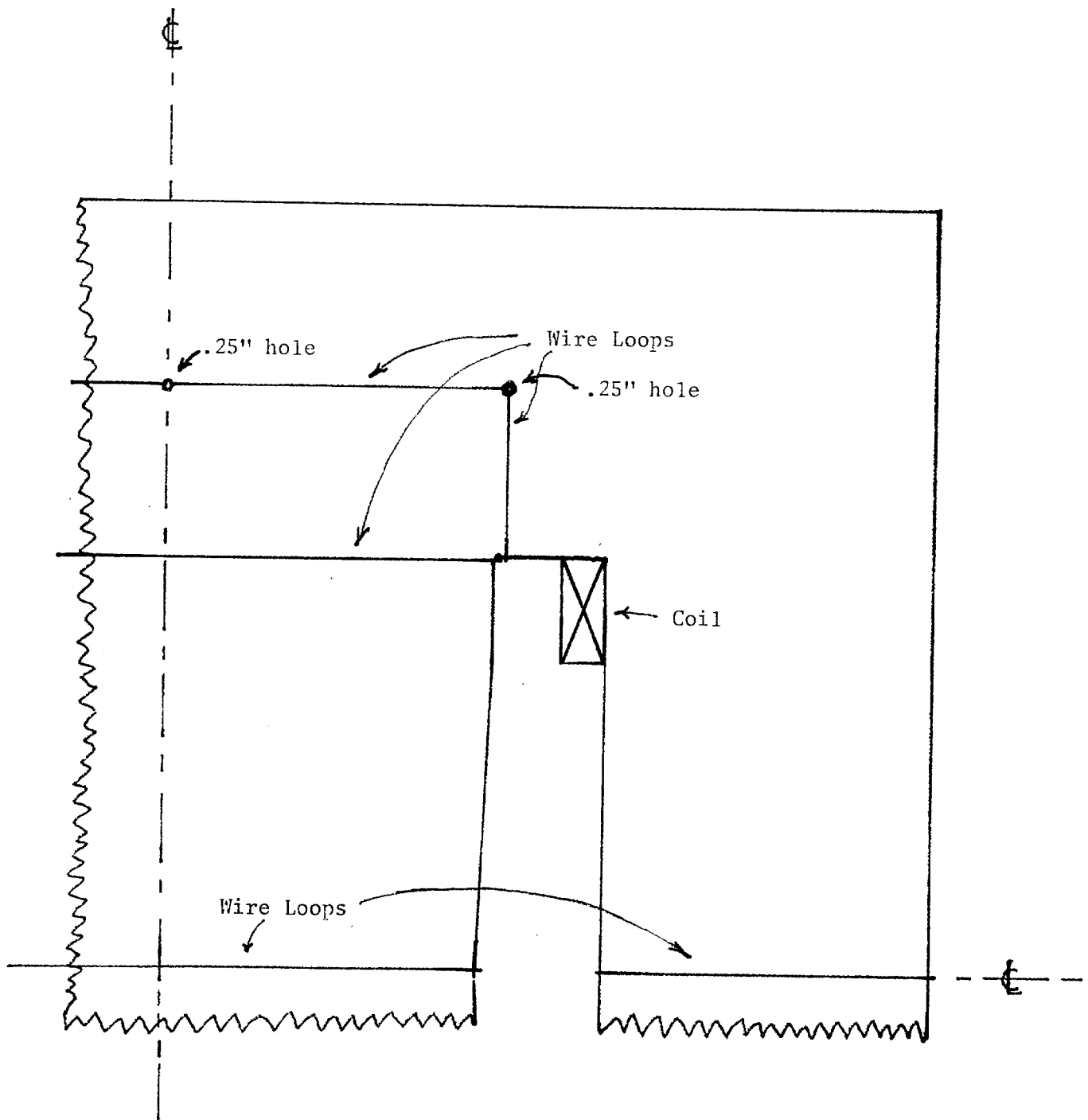


FIGURE A1. One quadrant of the magnet plate. The plate is symmetric about the two center lines. The overall dimensions are that of mill run "8 ft. steel plate 4" thick". The slots for the coils are "flame cut". The tapering of the inner edge of the coil slot is to improve the uniformity of the field in the central region. The wire loops were connected to voltage integrators and used to measure flux thru the surfaces they define.

APPENDIX B

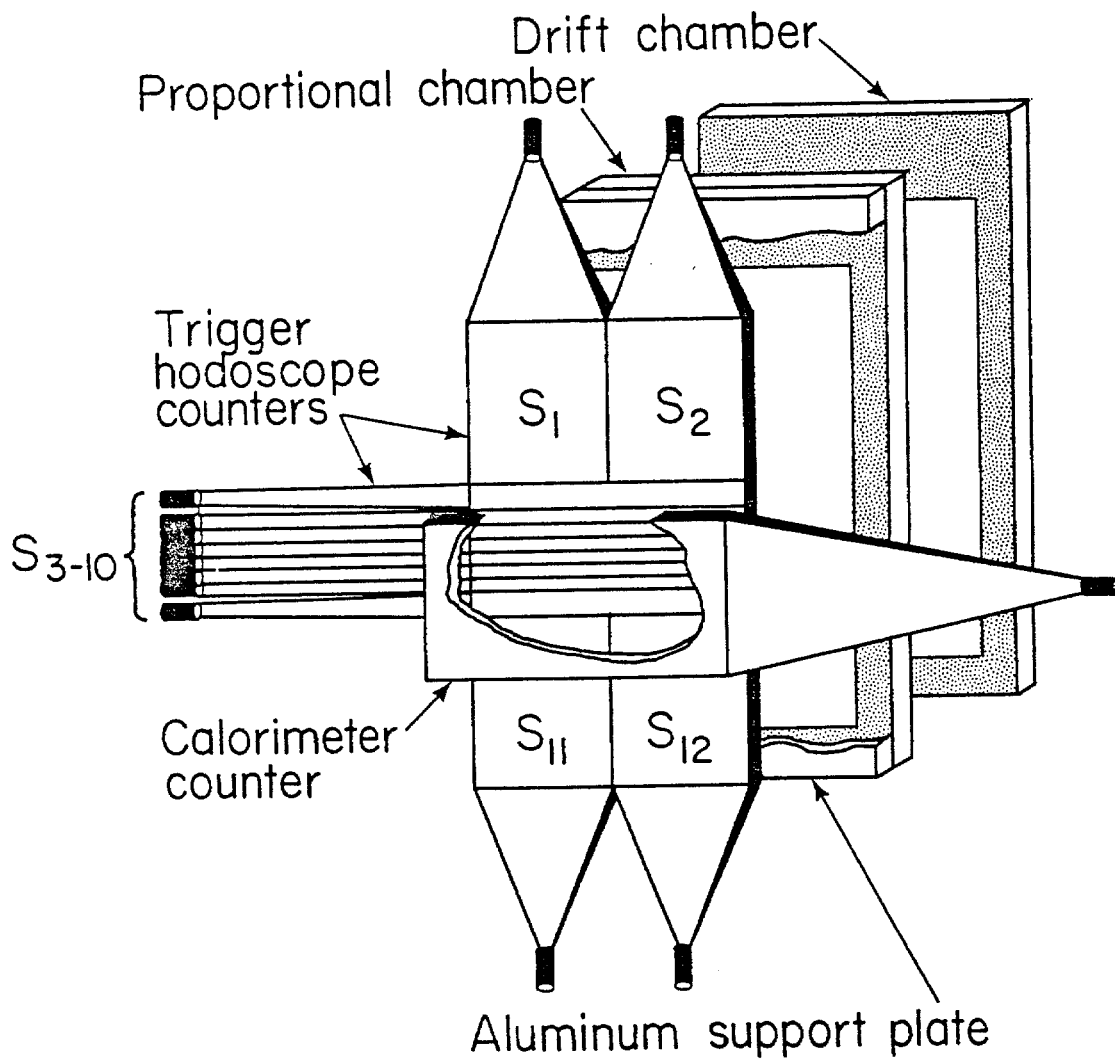
The experiment will use the same 19 multiwire proportional chambers (with modifications) which operated successfully during the E203/391 run. Each MWPC has an active area of $1.0 \times 1.8 \text{ m}^2$. A horizontal coordinate in the bendplane (x) is measured by one of 336 sense wires strung parallel to the long axis of the chamber with a 3.2 mm spacing. The vertical (z) and diagonal (u) coordinates are obtained from the corresponding pulses induced on the cathode planes, which are divided into horizontal or diagonal strips of 5.1 mm width (the cathode planes are actually made of wires spaced at 1.27 mm, with 4 wires tied together electrically to form 1 strip).

Since the induced pulses are rather broad and cover several strips, a special circuit is employed to electronically determine the center of each pulse. Each strip is connected to one input of a differential amplifier which is part of a network, as shown in Fig. B1. The induced charge produces an output pulse only from the one or two channels closest to the peak. This technique avoids the expense and complexity of having to digitize the pulse height on each induced channel, with a subsequent software interpolation to find the pulse center. An additional advantage of the induced pulse technique is that the transverse position of the induced pulse is determined solely by the sense-plane signal, such that no iterative corrections for track slope are necessary during track reconstruction.

During the E203/391 run, a "magic gas" mixture of 70% Argon, 23% Isobutane, 6.0% Methylal and 0.35% Freon 13B1 was used. The chambers were run for >2000 hours and were exposed to $>4 \times 10^{11}$ incident muons with no apparent deterioration in performance. The only problem with the chambers' performance was a drop in the efficiency of the induced planes in the beam area during periods of high beam flux - presumably due to space-charge effects.

One of the chambers has been returned to LBL and was opened for inspection. The chamber looked quite clean, with no sign of any deposits on the wires. The chamber has been reassembled and will be used to study various gas mixtures which would improve performance (lower operating voltage and/or improved efficiency in the beam area).

Other options which are being studied to improve system performance are increased electronic gain and the possibility of adding to each module a small 3-sense-plane proportional chamber which would cover the beam area. This last option would result in an improved vertical resolution over the present chambers, which would be useful with the smaller size of the new muon beam. Such chambers may also prove to be attractive as part of a redesigned trigger system.



XBL 795-1602

Figure 12. Exploded view of detectors within a typical gap between magnet modules.

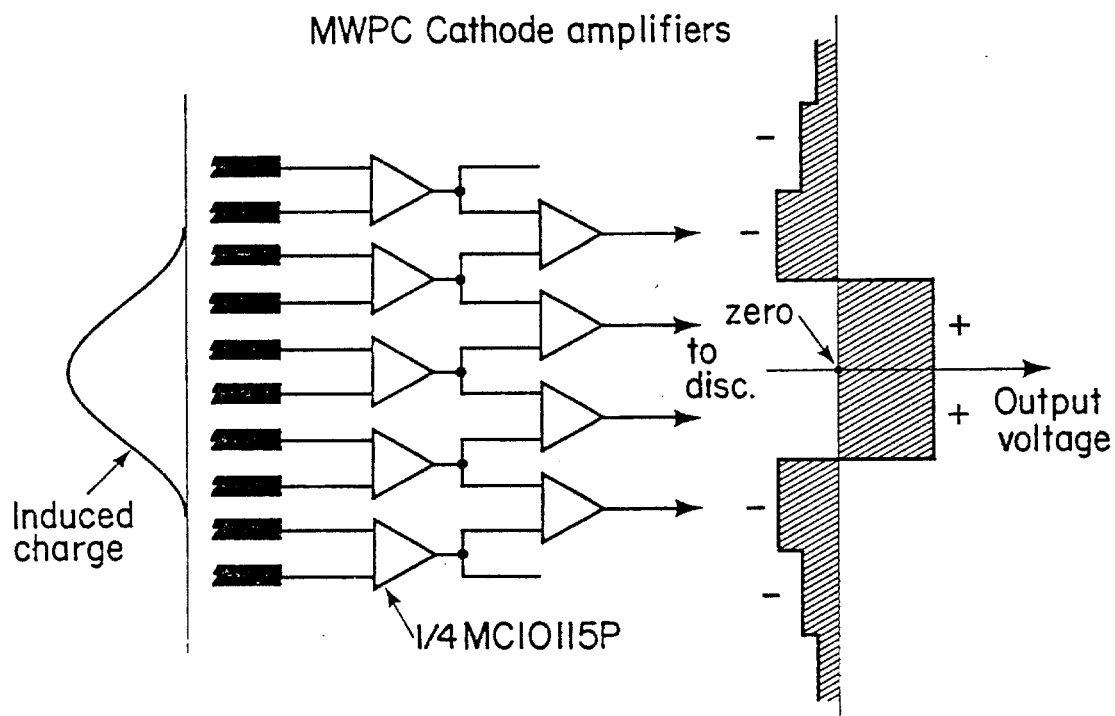
Table 2

Trigger Requirements for ≥ 1 , ≥ 2 , and ≥ 3
Final States

| <u>Final States</u> | <u>Requirement in each of 3 consecutive trigger banks</u> | <u>Requirement in Calorimeter</u> | <u>Measured Rate at 210 GeV per incident μ</u> |
|---------------------|---|--|---|
| $\geq 1\mu$ | $A \cdot \bar{B}$ ^a | None | 3×10^{-6} |
| $\geq 2\mu$ | ≥ 2 in A or B | ≥ 20 GeV ≥ 2 modules upstream | 7×10^{-6} |
| $\geq 3\mu$ | ≥ 3 in A or B | None | 13×10^{-6} |

^a "B" refers to S_3 - S_{10} in Figures 11 and 12;

"A" refers to S_1 , S_2 , S_{11} , and S_{12} .



XBL 795-1599

Figure B1. Network of differential amplifiers sensing the center of the charge distribution induced on proportional-chamber cathode strips. The outputs feed conventional MWPC discriminators. If the cathode-strip spacing is \sim half the plane spacing, one or two channels register with \sim equal probability, providing a vernier position measurement.

APPENDIX C

SUMMARY OF PREP EQUIPMENT USED IN E203

| <u>ITEM</u> | <u>NUMBER</u> |
|--------------------------------------|---------------|
| NIM Bin | 18 |
| NIM Power Supply | 18 |
| Quad Discriminator | 18 |
| Octal Discriminator | 12 |
| Dual 4-fold Logic Unit | 4 |
| Dual 4-fold Majority Logic Unit | 15 |
| Dual Updating Logic | 1 |
| Strobed Coincidence Unit | 4 |
| Multiplicity Logic | 9 |
| 2-Fold Logic Unit | 8 |
| Logic Fanin/Fanout | 36 |
| 4-fold Logic Fanout | 16 |
| Fan In | 1 |
| Linear Fanin/Fanout | 5 |
| Gate Generator | 2 |
| Visual Scaler | 2 |
| Preset Scaler | 1 |
| NIM Predet Box | 1 |
| Level Adapter | 4 |
| Camac Crate | 5 |
| Camac Power Supply | 5 |
| Dataway Display | 1 |
| Visual Branch Terminator | 1 |
| Branch Highway Cables | 7 |
| Camac Quad Scalars | 19 |
| 16 Channel Discriminator-Coincidence | 8 |
| 16 Channel Coincidence Register | 7 |
| Coincidence Registers | 8 |
| Differential ADC | 1 |
| Camac ADC | 13 |
| Camac Crate Controller | 5 |
| Visual Crate Controller | 1 |
| Output Register | 2 |
| Camac Predet | 1 |
| Camac Power Supply Alarm | 3 |
| X-Y Display Scope | 1 |
| Storage Scope | 2 |
| Dual Trace Units | 3 |
| Dual Time Base | 2 |
| High Voltage Power Supply (3kV) | 15 |
| Negative MWPC Supply | 12 |
| HV Distribution Box | 12 |
| Multiplexer | 1 |
| High Voltage Probe | 1 |
| NIM Cooling Fan | 14 |
| MRD Interface Cable | 1 |
| Memory/Raster Unit | 1 |

VII. Conclusions

The multimMuon spectrometer is a unique detector for the study of high energy muon interactions. It can be run in the new muon beam without significant modification. The software developed for E203/391 can be used immediately so that physics results can be available shortly after the beam turns on.

The spectrometer is uniquely suited to the study of multimMuon physics and there is no detector with comparable capability at Fermilab or CERN. With the new muon beam, this experiment can carry out an extremely valuable program even before the Tevatron is commissioned.

References

1. See for example, E. Derman and W. Marciano, *Ann. Phys.* 121 (1979); C.H. Llewellyn-Smith and E.H. Wiik, DESY 77/38; R.N. Cahn and F.J. Gilman, *Phys. Rev.* D17, 1313 (1978), and references contained in these works.
2. S. Weinberg, *Phys. Rev. Lett.* 19, 1264 (1967).
3. C.Y. Prescott et al., *Phys. Lett.* 84B, 524 (1979); C.Y. Prescott et al., *Phys. Lett.* 77B, 347 (1978).
4. J. Bartels, *Nucl. Phys.* B82, 172 (1974).
5. L.S. Rochester, et al., *Phys. Rev. Lett.* 36, 1284 (1976).
6. F. Wilczek, private communication.
7. L.F. Abbott, W.B. Atwood, and R. Michael Barnett, SIAC-PUB-2400, submitted to *Physical Review D*.
8. A.J. Buras, Fermilab-Pub-79/17-THY (unpublished).
9. A.R. Clark et al., invited paper presented by M. Strovink at the International Symposium on Lepton and Photon Interactions at High Energies, August 23-29, 1979 and LBL-9912.
10. A.R. Clark et al., *Phys. Rev. Lett.* 43, 189 (1979).
11. V. Barger, W.Y. Keung, and R.J.N. Phillips, *Phys. Rev.* D20, 630 (1979).
12. H. Fritzsch and K.H. Streng, *Physics Letters* 72B, 385 (1978).
13. J.J. Aubert et al., *Phys. Lett.* 89B, 267 (1980).
14. A.R. Clark et al., submitted to *Phys. Rev. Letters*.
15. A.R. Clark et al., to be submitted to *Phys. Rev. Letters*.
16. G. Gollin, M.V. Isaila, F.C. Shoemaker, and P. Surko, *IEEE Trans. Nucl. Sci.* NS-26, 59 (1979).
17. A. Malensck and M. Mugge, private communication.
18. See for example, F.E. Taylor et al., *IEEE Trans. Nucl. Sci.* NS-27, 30 (1980).
19. M.A. Beg et al., *Phys. Rev. Lett.* 38, 1252 (1977).

APPENDIX A

MAGNET DESIGN, CONSTRUCTION AND MEASUREMENT

Design

The design objectives were to generate as high a field as feasible (19 to 20 kG) in the fiducial region ($1.8 \times 1.0 \text{ m}^2$) of the spectrometer. In addition, relative uniformity over the central $1.2\text{m} \times 1.0 \text{ m}$ region is desirable to reduce the computing time of the data analysis. The coil configurations were constrained by the need of access for the calorimeter and trigger counters as well as the desire to use $.825" \times .625"$ copper conductor already in stock at Fermilab. A constraint from economics considerations required that mechanical tolerances on the magnet plates be compatible with standard mill run plate and "flame cutting" fabrication (2 mm).

The computer program TRIM¹ was used to calculate the magnetic field for various configurations of coils and plate size and shape. This program calculates the vector potential for a two dimensional field using a relaxation technique. The permeability of the iron is assumed to be a function of $|\vec{H}|$ and is entered in tabular form.

The most important contribution to uniformity in the central portion of the magnet was found to be from field lines that crossed the coil "slots" between the upper and lower coil. This effect was minimized by tapering the edge of the coil slot nearest the active region of the magnet. This configuration is shown in Fig. A1.

Construction

The plates were fabricated from mill run steel plate (AISI 1010). The coil slots were cut by the fabricator using a computer controlled flame cutting machine. The 91 plates were supplied by the mill from 5 different "heats". The "heat" from which each plate was fabricated was recorded. Samples of each "heat" were supplied by the vendor. The magnetic properties of these samples were measured at LBL².

As the plates were delivered to Fermilab their thickness and overall dimensions were recorded. Measurements of "bow" and "crown" were also recorded. These data with the magnetic data were used to order the plates in the spectrometer so that each 5 plate module would have similar overall dimensions on the average, as well as similar average magnetic permeability.

The plates were erected on concrete piers. They were positioned by a surveying technique that positioned the mean location of the four outer corners of the coil slots.

Operation

The magnet was operated at 4000 amperes (72000 ampere turns). To avoid any high order effects from eddy currents created during excitation of the magnet, a control circuit was used that changed the magnetic field during turn on or off at a uniform rate of ~ 300 gauss per second. This ensures that the \vec{H} field at the center of one of the plates lags the field at the surface by no more than 2 to 3 oersteds. The magnet was always excited by first turning it on to the opposite polarity first and then bringing it to the desired polarity using the above mentioned control.

Field Measurements

In addition to the B-H measurements of the steel (mentioned above) two sets of measurements of the field were made on the completed spectrometer. Thirteen loops of wire were inserted in each 5 plate module of the magnet as it was constructed. These loops were connected to voltage integrators. The signals from the integrators recorded the flux charge thru 13 different surfaces in each of the modules. The position of the loops is shown in Fig. A1.

The voltages from the integrators were recorded for a complete reversal of the magnetic field. These signals give a measure of the flux around the entire boundary of the fiducial region as well as a measurement of any left-right or up-down asymmetry. The precision and reproducibility of these measurements was one part in 2000. These measurements showed each module to be 4 fold symmetric to $\sim 0.1\%$.

These measurements were used to determine the absolute normalization of the average field in each module. The modules vary in average field by $\sim \pm 0.3\%$ with the first and last module higher by 1%. The first is due to differences in the total thickness of the various modules and the latter is because of the effect of the coil crossing the surface of the end modules.

These flux measurements were also used to determine the value of \vec{A} at specified points on the periphery of the fiducial region. These points were used as boundary conditions for the aforementioned TRIM program. The boundary conditions between these points were then adjusted until the TRIM program reproduced the field measured in the gaps between plates. In an ideal system \vec{H} in those gaps is equal to \vec{H} in the plate. This agreement could be found to $\sim 0.2\%$ of the absolute value of \vec{B} and the major component of \vec{B} . This represents an error in the direction of \vec{B} of less than 10 milliradians.

This approach to interpolating the shape of the field ensures that the interpolation between measured points satisfy Maxwell's Equations*. The final results were in good agreement with the predicted design field ($\sim 1\%$) except in the region very near the coil where the field changes very rapidly. We estimate the error of the measured fields to be $\sim 0.2\%$ in the fiducial region.

*It is interesting to note that since $|\vec{B}|$ is not a linear function of $|\vec{H}|$ the $\nabla \times \vec{B}$ in the magnet is not zero.

References

1. John B. Colonias, Particle Accelerator Design: Computer Programs, New York Academic Press (1974).
2. Don Nelson, Engineering Note MT-260, May 24, 1977.